

1
2
3
4
5
6
7
8
9
10
11
12
13
14
15
16
17
18
19
20
21
22
23
24
25
26
27
28
29
30
31
32
33
34
35
36
37
38
39
40
41
42
43
44
45
46
47
48
49
50
51
52
53
54
55
56
57
58
59
60

Highly Transparent Singlet Fission Solar Cell with Multi-Stacked Thin Metal Contacts for Tandem Applications

Ju Min Lee[†], Moritz H. Futscher[†], Luis M. Pazos-Outón[‡], and Bruno Ehrler^{†}.*

AUTHOR ADDRESS

[†] Center for Nanophotonics, AMOLF, Science Park 104, 1098 XG, Amsterdam, The Netherlands.

[‡] Electrical Engineering & Computer Sciences Dept., University of California, Berkeley, CA 94720-1770 United States.

AUTHOR EMAIL ADDRESS: Bruno Ehrler, b.ehrler@amolf.nl.

Keywords: Solar cell, Small molecule semiconductor, Singlet fission, Transparent electrode, Tandem solar cell.

1
2
3 ABSTRACT:
4
5
6

7 Singlet fission solar cells combined with silicon photovoltaics allow the construction of parallel
8 tandem solar cells, which benefit from better usage of high-energy photons. A key limiting factor
9 for the performance of such a tandem configuration is the transparency of the singlet fission front
10 cell. Here we show highly transparent singlet fission solar cells with a top contact of thin Ca:Ag
11 blends. The optimized contact leads to 81% average solar cell transmittance in the near-infrared
12 while maintaining more than half the short-circuit current density compared with an opaque
13 device. We simulate the performance of the parallel tandem stack, and assess the improvements
14 needed to fully realize the potential of singlet fission in this device configuration.
15
16
17
18
19
20
21
22
23
24
25
26
27
28
29
30
31
32
33
34
35
36
37
38
39
40
41
42
43
44
45
46
47
48
49
50
51
52
53
54
55
56
57
58
59
60

1
2
3 Charge carrier multiplication in solar cells allows the extraction of more than one charge
4 carrier per absorbed photon.[1] This multiplication effect increases the theoretical power
5 conversion efficiency (PCE) limit from 34 % to 45%.[2],[3] One of the most promising carrier
6 multiplication mechanisms is a process known as singlet fission, where a spin-singlet exciton,
7 generated by the absorption of a high-energy photon, spontaneously converts into two triplet
8 excitons with half of the original singlet exciton energy. Small molecule organic semiconductors,
9 such as pentacene, facilitate very high singlet exciton to triplet exciton conversion yields,
10 approaching 200 %.[4],[5],[6] Thus, in configurations where these triplet excitons can be
11 extracted, the photocurrent of the device can be increased.[7] One implementation of singlet
12 fission based solar cells are parallel-connected tandem devices, where the singlet fission cell acts
13 as the high-bandgap front cell in conjunction with a narrow-bandgap solar cell. Down-
14 conversion via singlet fission facilitates voltage-matching between the high- and low-bandgap
15 sub-cells. Recently, we demonstrated such a parallel connected tandem solar cell based on
16 pentacene and crystalline silicon.[8] Such voltage-matched parallel connected tandem solar cells
17 show more stable performance under a change of solar spectrum compared with the most
18 common current matched series-connected tandem devices. However, parallel tandem solar cells
19 did not achieve a high power conversion efficiency so far due to optical losses at the front solar
20 cell. Ideally the front cell would absorb all photons above the bandgap of the singlet fission
21 material, and be perfectly transparent at energies below that bandgap to maximize the number of
22 harvested photons in the back cell. Therefore, the performance of the tandem stack is crucially
23 determined by the transparency of the singlet fission front cell.

24
25 Here we investigate highly transparent, inverted pentacene solar cells with two transparent
26 contacts, an ITO bottom contact and a thin metal layer stacked top contact. The semiconducting
27
28
29
30
31
32
33
34
35
36
37
38
39
40
41
42
43
44
45
46
47
48
49
50
51
52
53
54
55
56
57
58
59
60

1
2
3
4
5
6
7
8
9
10
11
12
13
14
15
16
17
18
19
20
21
22
23
24
25
26
27
28
29
30
31
32
33
34
35
36
37
38
39
40
41
42
43
44
45
46
47
48
49
50
51
52
53
54
55
56
57
58
59
60

singlet fission layer acts as a filter that absorbs high-energy photons, while being perfectly transparent to below bandgap radiation. Consequently, below bandgap transparency is critically limited by the near-infrared transparency of the electrodes in such devices. Therefore, we focus on the fabrication of a conductive and transparent top metal electrode. Indium tin oxide (ITO) is the most common material used for transparent contacts because of its remarkable optical transparency and electrical conductivity.[9] However, ITO deposition demands high power sputtering, which would decompose any underlying organic layer during the deposition process. Metal nanowire networks,[10],[11],[12] nano-meshes[13],[14] and carbon nano-structures based on carbon nanotubes[15],[16] and graphene[17] have shown sufficient optical transparency and electrical conductivity as a top electrode for semi-transparent organic solar cells. However, those nano-structured layers are assembled by wet chemical processing and thermal annealing to form a uniform and electrically conductive layer. A pre-deposited organic layer can be dissolved or degraded by solvents during those processes. Recently it was shown that multilayers of thin metals can lead to >90% of optical transparency with an electrical conductivity comparable to ITO.[18],[19],[20] This multilayer structure is easily prepared by a mild thermal evaporation process, which avoids the degradation of the underlying organic layers during the deposition. In spite of the advantages, multi-stacked metal electrodes are designed for hole-carrier collection, while conventional singlet fission based solar cells require electron extraction at the top electrode.

We introduce an inverted singlet fission based organic solar cell to incorporate the highly transparent multilayer electrode. The device architecture and energy band diagram of conventional and inverted singlet fission based organic solar cells are illustrated in **Figure 1(a)** and (b). For the conventional singlet fission cell we follow Congreve et al.,[6] using a

1
2
3 heterojunction between pentacene and C₆₀ fullerene with poly(3,4-ethylenedioxythiophene)
4 polystyrene sulfonate (PEDOT:PSS) / poly(3-hexylthiophene-2,5-diyl) (P3HT) as the hole
5 extraction layers. For the inverted cell we use molybdenum oxide (MoO_x) as the hole extraction
6 (top) layer and bathocuproine (BCP) and zinc oxide (ZnO) as the bottom electron extraction
7 layers. The current density - voltage (*J-V*) performance of opaque conventional and inverted
8 solar cells are shown in **Figure 1(c)** and summarized in the inset. The conventional cell shows a
9 short-circuit current density (*J_{SC}*) of 6.7 ± 0.3 mA/cm², which is higher than the *J_{SC}* of 5.1 ± 0.2
10 mA/cm² from the inverted cell. However, the inverted solar cell shows superior open-circuit
11 voltage (*V_{OC}*) of 0.40 ± 0.01 V and fill factor (FF) of 56 ± 2 % in comparison to the conventional
12 cell with a *V_{OC}* of 0.34 ± 0.01 V and a FF of 45 ± 1 %, resulting in 1.12 ± 0.1 % of average PCE.
13
14
15
16
17
18
19
20
21
22
23
24
25
26

27 The solar cell performance is significantly affected by the thickness of the pentacene layer. We
28 optimized the thickness of pentacene in the inverted solar cell from 20 to 100 nm to find the ideal
29 thickness, as shown in the *J-V* curves in **Figure 1(d)**. *J_{SC}* increases with the thickness from 20 to
30 100 nm. The enhanced absorption of the thicker pentacene layer presumably leads to higher
31 exciton generation rate while still allowing for most excitons to reach the pentacene/C₆₀
32 interface. The *V_{OC}* of the solar cells is also increased when the pentacene thickness is increased,
33 presumably because of voids forming in the thin pentacene films (see Supplementary
34 Information S2). At higher thicknesses, the *J_{SC}* and *V_{OC}* drop due to recombination in the
35 pentacene layer as the layer thickness exceeds the exciton diffusion length.[21],[22]
36
37
38
39
40
41
42
43
44
45
46
47
48 Additionally, the thicker layers (≥ 80 nm) led to less reproducible results, presumably due to the
49 rougher surface morphology of the thick layers (see Supplementary Information S2). In the
50 following we will use solar cells with 60 nm of pentacene.
51
52
53
54
55
56
57
58
59
60

1
2
3 To optimize the optical transparency of the pentacene solar cell for the tandem device
4 configuration, we introduced two different semi-transparent top electrodes composed of multi-
5 stacked metals replacing the conventional opaque metal electrode. Firstly, we simply reduced the
6 thickness of the Ag layer down to 10 nm. To achieve uniform Ag deposition we deposited 1 nm
7 of aluminum (Al) underneath of Ag as a seed layer. The transmittance of the semi-transparent
8 inverted pentacene solar cell with the thin Al/Ag contact is shown in **Figure 2(a)**. Upon reducing
9 the thickness of Ag from 70 to 10 nm the transmittance in the visible to near-infrared (NIR)
10 region (400-1100 nm) increases from 5 % to 40 %. To reduce the reflection from the top
11 electrode, we introduced 94 nm of molybdenum oxide (MoO_x) on top of the Al/Ag electrode as
12 an anti-reflection (AR, $\lambda/4 = 225$ nm) coating considerably enhancing the transmittance of the
13 device in the near-IR region (dashed lines in **Figure 2(a)**). **Figure 2(b)** shows the average
14 transmittance of the full device in the visible region (400 to 800 nm, T_{vis}) and the region below
15 the pentacene band gap which we call NIR region (700 to 1100 nm, T_{NIR}) as a function of Ag
16 layer thickness. The transmittance continuously decreases with top contact thickness. With the
17 AR coating both T_{NIR} and T_{vis} are enhanced by 5 - 15 %. The sheet resistance (R_S) of the contact
18 has to be considered for efficient charge collection in a solar cell. Ag contacts of all thicknesses
19 without AR coating present R_S below $6 \Omega/\square$ except for the 10 nm Ag contact with much larger
20 R_S of $127 \Omega/\square$ (see **Figure 2(c)**), presumably because of the formation of unconnected Ag
21 domains.[19]
22
23
24
25
26
27
28
29
30
31
32
33
34
35
36
37
38
39
40
41
42
43
44
45
46
47

48 The second semi-transparent multilayer metal contact we apply is a blend of calcium and silver
49 (Ca:Ag). Schubert et al. showed that this combination of materials exhibits an unusually high
50 optical transmittance, while maintaining good conductivity.[20],[23] We sequentially deposited 1
51 nm of Al and Ag seed layers on top of the solar cell structure to achieve a uniform Ca:Ag layer.
52
53
54
55
56
57
58
59
60

1
2
3 Ca and Ag were co-evaporated to form a blend that self-assembles as a Ag network surrounded
4 by a Ca shell.[23] **Figure 2(d)** shows the transmittance of semi-transparent solar cells with
5 varying Ca:Ag thicknesses. All devices with Ca:Ag electrodes show superior transmittance,
6 almost 30 % higher over the entire wavelength range in comparison to devices with the same
7 thickness of thin Ag electrode. As an AR coating we used 90 nm of tris(8-
8 hydroxyquinolino)aluminium (Alq₃) on top of the Ca:Ag electrode, following Schubert et
9 al.[23] (dashed line in **Figure 2(d)**). The AR coating is designed to maximize T_{NIR} ($\lambda/4 = 200$
10 nm) and thus decreases the T_{vis}, while T_{NIR} is enhanced by around 10 % for all Ca:Ag
11 thicknesses. The AR layer enhanced the transparency of the solar cell in the 700 to 1100 nm
12 region even more significantly compared to the thin Ag electrode. The device with 10 nm of
13 Ca:Ag electrode with AR coating achieved the maximum transmittance of 92 % at 820 nm. T_{vis}
14 and T_{NIR} are decreasing with increasing Ca:Ag layer thickness, but with a much weaker thickness
15 dependence compared to the thin Ag electrode (**Figure 2(b)** and (e)). The thickness of the Ca:Ag
16 layer also determines the electrical performance, and in the following we optimize the solar cell
17 for best overall performance. The MoO_x/Al/Ag/Ca:Ag structure shows higher R_S than the
18 MoO_x/Al/thin Ag for all layer thickness (see **Figure 2(f)**). 40 nm of Ca:Ag contact allows 29
19 Ω/\square of R_S with 60 % of T_{NIR}, which is comparable to the 22 Ω/\square of our commercial ITO (125
20 nm), whereas it sharply increases to 140 Ω/\square at 10 nm of Ca:Ag contact, unfavorable for solar
21 cell operation. We note that the resistance of our Ca:Ag contact is higher than reported
22 previously for this electrode,[23] presumably because the surface roughness of the underlying
23 active layer is larger (see Supplementary Information S2).
24
25
26
27
28
29
30
31
32
33
34
35
36
37
38
39
40
41
42
43
44
45
46
47
48
49
50
51

52
53 *J-V* characteristics of semi-transparent solar cells with thin Ag and Ca:Ag electrodes of
54 varying thickness are shown in **Figure 3(a)** and (b), respectively. A semi-transparent solar cell
55
56
57
58
59
60

1
2
3 with a thin Ag (40 nm) electrode 0.90 % of PCE, shows a performance of only slightly less than
4 the opaque solar cell (**Figure 3(a)**, full solar cell details in Supplementary Information Table S3).
5
6 The solar cell performance is almost identical with and without the AR coating (Supplementary
7 Information S4). When the Ag thickness is reduced to 20 nm to yield higher transmission (T_{NIR}
8 of 40 %) the solar cell performance is considerably reduced (PCE 0.45%), mostly due to a lower
9 J_{SC} of 2.5 mA/cm². The Ca:Ag electrode allows for much higher T_{NIR} values for comparable
10 solar cell efficiencies. The AR coated semi-transparent solar cell with a 50 nm thick Ca:Ag
11 electrode presents 3.0 mA/cm² of J_{SC} , and a PCE to 0.64 % at 54 % of T_{NIR} (see **Figure 3(b)**). An
12 extremely transparent solar cell with only 20 nm Ca:Ag layer shows 81 % of T_{NIR} while
13 maintaining 2.3 mA/cm² of J_{SC} , yielding 0.50 % of PCE. We note that the reduction in J_{SC} in the
14 transparent solar cell is mostly because of the absence of a reflective silver contact. The
15 reflection of the silver contact allows designing the organic solar cell as a Fabry-Perot cavity,
16 leading to much stronger absorption in the pentacene layer.[24] Transparent solar cells thus
17 require materials with large triplet exciton diffusion length or selective reflectivity of the contact.
18
19 **Figure 3(c)** summarizes the J_{SC} as a function of T_{NIR} with the two types of electrodes. The
20 Ca:Ag layer yields nearly 20 % higher T_{NIR} for the same J_{SC} value than solar cells based on the
21 Al/Ag contact. J_{SC} continuously decreases to half the value of the opaque device at 70 % of T_{NIR}
22 owing to lower conductivity and reduced reflection off the back contact. V_{OC} and FF are almost
23 identical for all contact thicknesses > 10 nm.
24
25
26
27
28
29
30
31
32
33
34
35
36
37
38
39
40
41
42
43
44
45
46
47

48 Semi-transparent singlet fission solar cells can be used as the front cell of a tandem device
49 configuration in combination with a Si back cell. Singlet fission allows the connection of devices
50 in a two-terminal parallel cell (**Figure 4(a)**), ensuring higher spectral stability compared to
51 conventional, series connected tandem cells[8] while maintaining the two-terminal advantage
52
53
54
55
56
57
58
59
60

1
2
3 compared to four-terminal cells (**Figure 4(b)**). In the following we calculate the potential singlet
4 fission/Si tandem solar cell efficiency based on the transmittance spectrum and the performance
5 of the semi-transparent singlet fission front cells with different Ca:Ag thicknesses (see
6 Supplementary Information S6 for details of the simulation).[25] **Figure 4(c)** shows the
7 calculated J_{SC} of parallel tandems made from the singlet fission cells together with the record
8 performing silicon solar cell.[26] A thick Ca:Ag contact enhances the J_{SC} of a semi-transparent
9 front cell by lowering the R_S . However, more serious photon absorption and reflection at the
10 thick electrode reduces the J_{SC} of the Si back cell. The J_{SC} of the parallel tandem solar cell is
11 maximized at 32.6 mA/cm² for 15 nm of Ca:Ag contact thickness (**Figure 4(d)**). However, the
12 tandem solar cells do not yield performances higher than the Si bottom cell alone, even with the
13 highly transparent front cell obtaining >80 % of T_{NIR} . To achieve a tandem cell performance
14 higher than the two individual sub-cells, the current of the front cell needs to be higher than the
15 current loss from placing it in front of the silicon cell. In the final device configuration, the
16 silicon and the singlet fission cell might share a common ITO contact. Some silicon cells already
17 feature ITO contacts,[27] and the singlet fission cell could simply be placed on top. The AR
18 coating of the Si cell would then need to be placed on top of the singlet fission cell. Thus, the
19 absorption at the active layer of the singlet fission front cell needs to be maximized to benefit
20 from carrier multiplication, while maintaining above unity quantum efficiency. In addition, the
21 parallel tandem solar cell shows lower PCE in comparison to the four-terminal tandem because
22 of the large voltage difference between the maximum power point (V_{mpp}) of the semi-transparent
23 pentacene device and the Si solar cell (see Supplementary Information Figure S6). V_{mpp} matching
24 is required in order to maximize the performance of parallel connected tandem solar cells. For
25 this reason, singlet fission cells based on materials with a higher triplet energy (such as
26
27
28
29
30
31
32
33
34
35
36
37
38
39
40
41
42
43
44
45
46
47
48
49
50
51
52
53
54
55
56
57
58
59
60

1
2
3 tetracene), and thus larger voltage, would greatly benefit the tandem solar cell performance.
4
5 However, in our hands, as well as in the literature, tetracene based singlet fission solar cells have
6
7 shown lower quantum efficiency than pentacene cells,[28] despite the quantitative singlet fission
8
9 in tetracene under optimized conditions.[29],[30],[31] This illustrates the requirement for
10
11 optimizing device architecture, interfaces, and tetracene growth. Furthermore, the series
12
13 resistance of the singlet fission solar cell is high in comparison with the Si solar cell, which
14
15 degrades the FF of the parallel tandem (see Supplementary Information S2).
16
17
18
19

20 In summary, we have demonstrated semi-transparent pentacene solar cells introducing a
21
22 highly transparent top contact, which could be used to sensitize a silicon solar cell or other low-
23
24 bandgap cells in a parallel tandem configuration. We introduce an inverted singlet fission solar
25
26 cell architecture, designed to allow for the transparent electrode, which achieves 1.21 % of PCE,
27
28 higher than 1.03 % of conventional, non-inverted singlet fission solar cells. We characterize the
29
30 inverted solar cells with thin Al/Ag and Al/Ag/Ca:Ag multi-stacked metals as a transparent
31
32 electrode with various electrode thicknesses. Thin Ag shows low sheet resistance (below $6 \Omega/\square$)
33
34 while the Ca:Ag blend layer leads to a high optical transparency (e.g. 48 % of T_{NIR} with $28 \Omega/\square$
35
36 sheet resistance). Furthermore, deposition of an anti-reflection layer on Ca:Ag enhanced the T_{NIR}
37
38 of the solar cell. The J - V characteristics of semi-transparent solar cells were mainly determined
39
40 by the thickness of the transparent top contact. In particular, the cell with a 20 nm Ca:Ag contact
41
42 showed more than half the J_{SC} of the opaque solar cell, with 81 % T_{NIR} . Finally, we calculate the
43
44 efficiency of a parallel tandem configuration consisting of our semi-transparent singlet fission
45
46 front cells together with a Si back cell, absorbing high- and low-energy photons, respectively.
47
48 The compromise between transmittance and performance of the front cell determined the J_{SC} of
49
50 the tandem configuration, resulting in a maximum J_{SC} of 32.6 mA/cm^2 . However, reaching a
51
52
53
54
55
56
57
58
59
60

1
2
3 higher tandem performance than the Si cell alone is still challenging using the current semi-
4 transparent singlet fission front cells. Enhancing the absorption in the active layer is critical to
5
6 maximize carrier multiplication, especially for singlet fission materials with high triplet energy
7
8 to improve the V_{OC} of the singlet fission cell and the overall tandem performance.
9
10
11
12
13
14
15
16
17
18
19
20
21
22
23
24
25
26
27
28
29
30
31
32
33
34
35
36
37
38
39
40
41
42
43
44
45
46
47
48
49
50
51
52
53
54
55
56
57
58
59
60

For Peer Review

ACKNOWLEDGMENT

The authors acknowledge Marc Duursma for technical support and Eric Johlin for comments on the manuscript. This work is part of the research program of The Netherlands Organization for Scientific Research (NWO).

Supporting Information Available: We provide details about fabrication and characterization of the semi-transparent singlet fission solar cells and the model used to simulate the performance of singlet fission/Si tandem solar cells.

REFERENCES

- [1] Werner JH, Kolodinski S, Queisser HJ. Novel optimization principles and efficiency limits for semiconductor solar cells. *Phys Rev Lett* 1994;72:3851–4.
- [2] Shockley W, Queisser HJ. Detailed balance limit of efficiency of p-n junction solar cells. *J Appl Phys* 1961;32:510–9. doi:10.1063/1.1736034.
- [3] Hanna MC, Nozik AJ. Solar conversion efficiency of photovoltaic and photoelectrolysis cells with carrier multiplication absorbers. *J Appl Phys* 2006;100:74510.
- [4] Smith MB, Michl J. Singlet fission. *Chem Rev* 2010;110:6891–936. doi:10.1021/cr1002613.
- [5] Rao A, Wilson MWB, Hodgkiss JM, Albert-Seifried S, Bäessler H, Friend RH. Exciton fission and charge generation via triplet excitons in pentacene/C60 bilayers. *J Am Chem Soc* 2010;132:12698–703. doi:10.1021/ja1042462.
- [6] Congreve DN, Lee J, Thompson NJ, Hontz E, Yost SR, Reuswig PD, et al. External

- 1
2
3 Quantum Efficiency Above 100% in a Singlet-Exciton-Fission-Based Organic
4 Photovoltaic Cell. *Science* (80-) 2013;340:334–7.
5
6
7
8
9 [7] Ehrler B, Walker BJ, Böhm ML, Wilson MWB, Vaynzof Y, Friend RH, et al. In situ
10 measurement of exciton energy in hybrid singlet-fission solar cells. *Nat Commun*
11 2012;3:1019. doi:10.1038/ncomms2012.
12
13
14
15
16 [8] Pazos Outón LM, Lee JM, Futscher MH, Kirch A, Tabachnyk M, Friend RH, et al. A
17 Silicon-Singlet Fission Tandem Solar Cell Exceeding 100% External Quantum Efficiency
18 with High Spectral Stability. *ACS Energy Lett* 2017;2:476–80.
19 doi:10.1021/acsenergylett.6b00678.
20
21
22
23
24
25
26 [9] Bush KA, Bailie CD, Chen Y, Bowring AR, Wang W, Ma W, et al. Thermal and
27 Environmental Stability of Semi-Transparent Perovskite Solar Cells for Tandems Enabled
28 by a Solution-Processed Nanoparticle Buffer Layer and Sputtered ITO Electrode. *Adv*
29 *Mater* 2016;28:3937–43. doi:10.1002/adma.201505279.
30
31
32
33
34
35
36 [10] Hu L, Kim HS, Lee JY, Peumans P, Cui Y. Scalable coating and properties of transparent,
37 flexible, silver nanowire electrodes. *ACS Nano* 2010;4:2955–63. doi:10.1021/nn1005232.
38
39
40
41
42
43 [11] Chen CC, Dou L, Zhu R, Chung CH, Song T Bin, Zheng YB, et al. Visibly transparent
44 polymer solar cells produced by solution processing. *ACS Nano* 2012;6:7185–90.
45 doi:10.1021/nn3029327.
46
47
48
49
50 [12] Bailie CD, Christoforo MG, Mailoa JP, Bowring AR, Unger EL, Nguyen WH, et al. Semi-
51 transparent perovskite solar cells for tandems with silicon and CIGS. *Energy Environ Sci*
52 2015;8:956–63. doi:10.1039/C4EE03322A.
53
54
55
56
57
58
59
60

- 1
2
3
4
5
6
7
8
9
10
11
12
13
14
15
16
17
18
19
20
21
22
23
24
25
26
27
28
29
30
31
32
33
34
35
36
37
38
39
40
41
42
43
44
45
46
47
48
49
50
51
52
53
54
55
56
57
58
59
60
- [13] Bryant D, Greenwood P, Troughton J, Wijdekop M, Carnie M, Davies M, et al. A transparent conductive adhesive laminate electrode for high-efficiency organic-inorganic lead halide perovskite solar cells. *Adv Mater* 2014;26:7499–504. doi:10.1002/adma.201403939.
- [14] Sciacca B, Van De Groep J, Polman A, Garnett EC. Solution-Grown Silver Nanowire Ordered Arrays as Transparent Electrodes. *Adv Mater* 2016;28:905–9. doi:10.1002/adma.201504045.
- [15] Ago H, Petritsch K, Shaffer MSP, Windle AH, Friend RH. Composites of carbon nanotubes and conjugated polymers for photovoltaic devices. *Adv Mater* 1999;11:1281–5. doi:10.1002/(SICI)1521-4095(199910)11:15<1281::AID-ADMA1281>3.0.CO;2-6.
- [16] Kim YH, Müller-Meskamp L, Zakhidov AA, Sachse C, Meiss J, Bikova J, et al. Semi-transparent small molecule organic solar cells with laminated free-standing carbon nanotube top electrodes. *Sol Energy Mater Sol Cells* 2012;96:244–50. doi:10.1016/j.solmat.2011.10.001.
- [17] You P, Liu Z, Tai Q, Liu S, Yan F. Efficient Semitransparent Perovskite Solar Cells with Graphene Electrodes. *Adv Mater* 2015;27:3632–8. doi:10.1002/adma.201501145.
- [18] Kim H, Kim HS, Ha J, Park NG, Yoo S. Empowering Semi-Transparent Solar Cells with Thermal-Mirror Functionality. *Adv Energy Mater* 2016;6:1–9. doi:10.1002/aenm.201502466.
- [19] Schubert S, Meiss J, Müller-Meskamp L, Leo K. Improvement of transparent metal top electrodes for organic solar cells by introducing a high surface energy seed layer. *Adv*

- 1
2
3 Energy Mater 2013;3:438–43. doi:10.1002/aenm.201200903.
4
5
6
7 [20] Meiss J, Ziehlke H, Schubert S, Leo K, Riede M. Coevaporated calcium-silver metal
8 alloys as contact for highly transparent organic solar cells. Energy Sci Eng 2014;2:77–85.
9 doi:10.1002/ese3.34.
10
11
12
13
14 [21] Yoo S, Domercq B, Kippelen B. Efficient thin-film organic solar cells based on
15 pentacene/C 60 heterojunctions. Appl Phys Lett 2004;85:5427–9. doi:10.1063/1.1829777.
16
17
18
19
20 [22] Tabachnyk M, Ehrler B, Bayliss S, Friend RH, Greenham NC. Triplet diffusion in singlet
21 exciton fission sensitized pentacene solar cells. Appl Phys Lett 2013;103:4–8.
22 doi:10.1063/1.4824420.
23
24
25
26
27
28 [23] Schubert S, Müller-Meskamp L, Leo K. Unusually High Optical Transmission in Ca:Ag
29 Blend Films: High-Performance Top Electrodes for Efficient Organic Solar Cells. Adv
30 Funct Mater 2014;24:6668–76. doi:10.1002/adfm.201401854.
31
32
33
34
35
36 [24] Günes S, Neugebauer H, Sariciftci NS. Conjugated polymer-based organic solar cells.
37 Chem Rev 2007;107:1324–38. doi:10.1021/cr050149z.
38
39
40
41 [25] Futscher MH, Ehrler B. Efficiency Limit of Perovskite/Si Tandem Solar Cells. ACS
42 Energy Lett 2016;1:863–8. doi:10.1021/acsenergylett.6b00405.
43
44
45
46
47 [26] Green MA, Emery K, Hishikawa Y, Warta W, Dunlop ED, Levi DH, et al. Solar cell
48 efficiency tables (version 49). Prog Photovoltaics Res Appl 2017;25:3–13.
49 doi:10.1002/pip.2855.
50
51
52
53
54
55 [27] Knight MW, van de Groep J, Bronsveld PCP, Sinke WC, Polman A. Soft imprinted Ag
56 nanowire hybrid electrodes on silicon heterojunction solar cells. Nano Energy
57
58
59
60

1
2
3 2016;30:398–406. doi:<https://doi.org/10.1016/j.nanoen.2016.10.011>.

- 4
5
6 [28] Wu TC, Thompson NJ, Congreve DN, Hontz E, Yost SR, Van Voorhis T, et al. Singlet
7 fission efficiency in tetracene-based organic solar cells. *Appl Phys Lett* 2014;104:193901.
8 doi:<http://dx.doi.org/10.1063/1.4876600>.
- 9
10
11 [29] Burdett JJ, Bardeen CJ. Quantum Beats in Crystalline Tetracene Delayed Fluorescence
12 Due to Triplet Pair Coherences Produced by Direct Singlet Fission. *J Am Chem Soc*
13 2012;134:8597–607. doi:10.1021/ja301683w.
- 14
15
16 [30] Tayebjee MJY, Clady RGCR, Schmidt TW. The exciton dynamics in tetracene thin films.
17 *Phys Chem Chem Phys* 2013;15:14797–805. doi:10.1039/C3CP52609G.
- 18
19
20 [31] Piland GB, Bardeen CJ. How Morphology Affects Singlet Fission in Crystalline
21 Tetracene. *J Phys Chem Lett* 2015;6:1841–6. doi:10.1021/acs.jpcclett.5b00569.
- 22
23
24
25
26
27
28
29
30
31
32
33
34
35
36
37
38
39
40
41
42
43
44
45
46
47
48
49
50
51
52
53
54
55
56
57
58
59
60

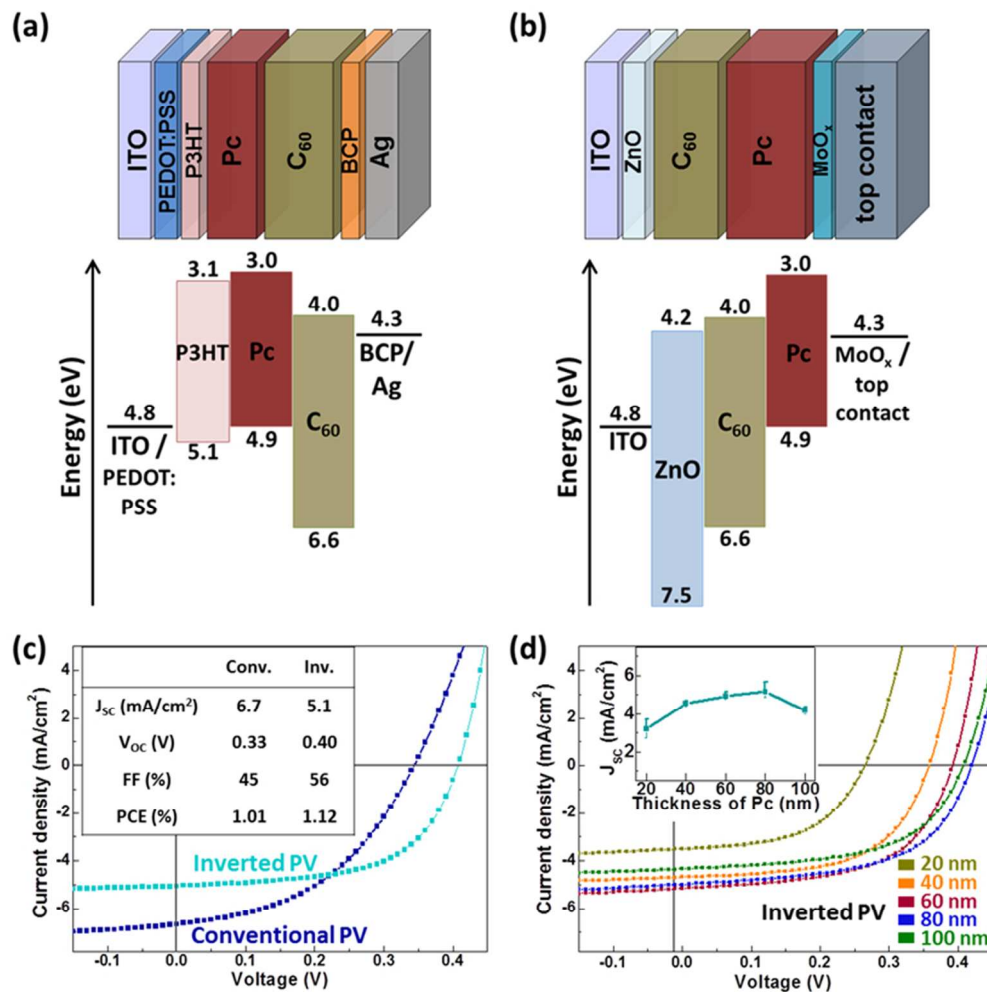
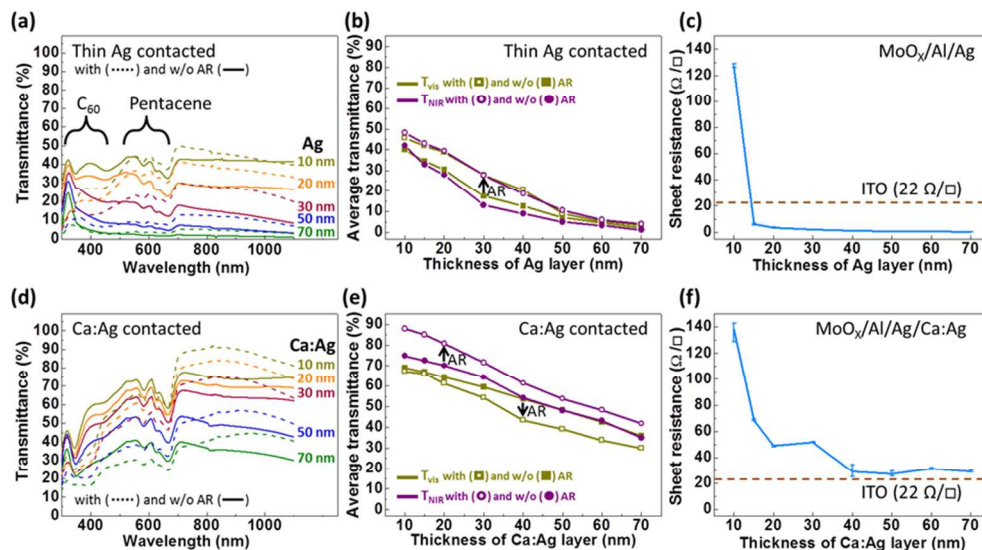


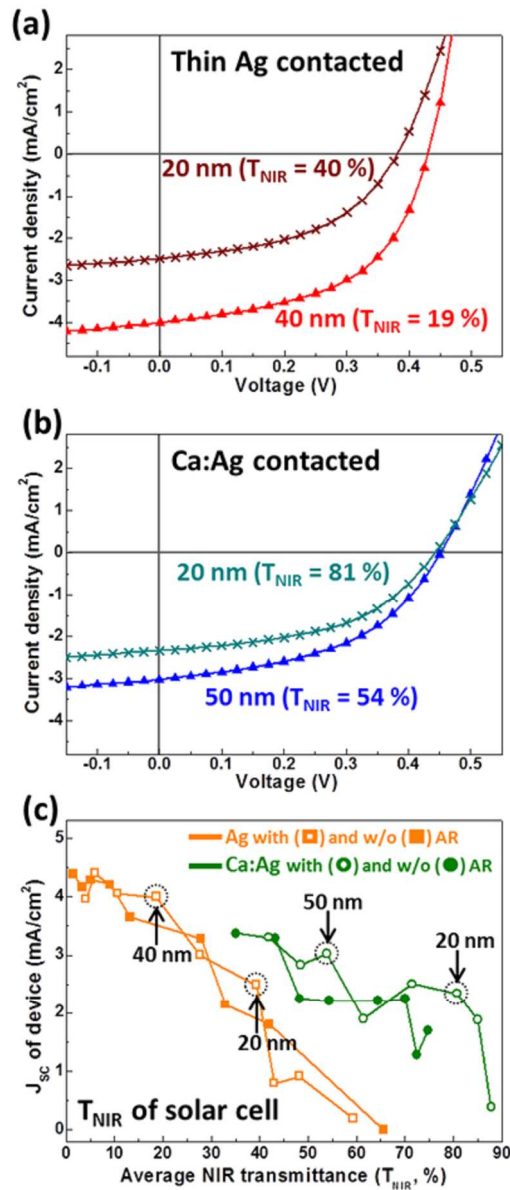
Illustration of the solar cell architecture and energy band diagram of (a) the conventional pentacene solar cell based on reference[6] and (b) the inverted solar cell with different top contact structures such as the opaque silver (100nm thick), transparent thin silver and transparent calcium:silver blended layer. (c) Current density-voltage (J - V) characteristics of conventional and inverted solar cells (d) J - V characteristics and short-circuit current density (J_{sc} , inset) of inverted solar cells with 20 to 100 nm of pentacene layer thickness.

139x140mm (150 x 150 DPI)



Optical transmittance of solar cell with different thickness of (a) thin Ag contact and (d) Ca:Ag contact. Brackets in (a) indicate mostly C₆₀ and Pentacene absorption. Calculated average transmittance of solar cell in visible (400 to 800 nm, T_{vis}) and near infrared (700 to 1100 nm, T_{NIR}) region with (b) thin Ag contact and (e) Ca:Ag contact with and without anti-reflection (AR) coating. Sheet resistance as a function of layer thickness of (c) Ag and (f) Ca:Ag without AR coating. The dashed lines shows the sheet resistance of our commercial ITO (125 nm).

165x92mm (150 x 150 DPI)



J-V characteristics of semi-transparent solar cells with (a) thin Ag contact and (b) Ca:Ag contact. (c) J_{sc} of semi-transparent solar cells with the two types of top contact as a function of T_{NIR} for solar cells with and without AR coating.

219x505mm (96 x 96 DPI)

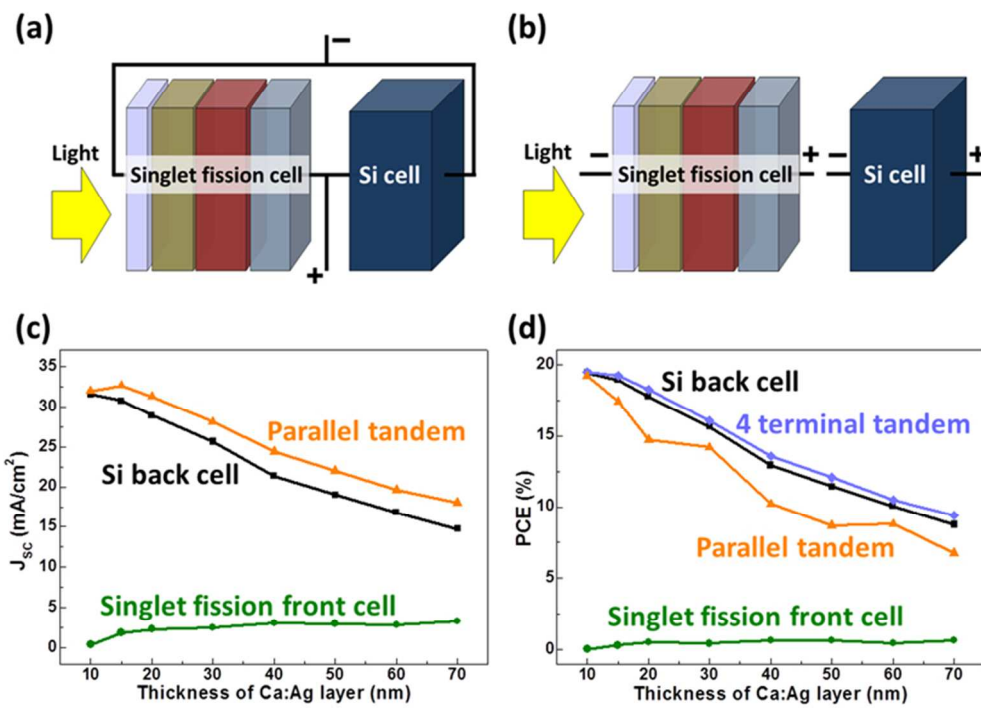


Illustration of tandem configuration based on semi-transparent singlet fission front and silicon back cells. Sub-cells are electrically connected in (a) parallel and (b) four-terminal. (c) Calculated J_{sc} and (d) PCE of singlet fission/Si tandem solar cells from our transparent pentacene cells with different Ca:Ag layer thicknesses.

140x103mm (150 x 150 DPI)